

Focused high- and low-energy ion milling for TEM specimen preparation

A. Lotnyk*, D. Poppitz, U. Ross, J.W. Gerlach, F. Frost, S. Bernütz, E. Thelander, B. Rauschenbach

Leibniz Institute of Surface Modification (IOM), Permoserstr. 15, D-04318 Leipzig, Germany

ARTICLE INFO

Article history:

Received 22 May 2015

Received in revised form 30 June

2015 Accepted 1 July 2015

Available online 8 July 2015

Keywords:

TEM specimen preparation

Focused low-energy ion milling

Thin films

Interfaces

GaN

Phase change materials

ABSTRACT

For atomic-resolution aberration-corrected (Cs-corrected) scanning transmission electron microscopy (STEM) the quality of prepared TEM specimens is of crucial importance. High-energy focused gallium ion beam milling (FIB) is widely used for the production of TEM lamella. However, the specimens after conventional FIB preparation are often still too thick. In addition, damage and amorphization of the TEM specimen surface during the milling process occur. In order to overcome these disadvantages, low-energy Ar ion milling of FIB lamellae can be applied. In this work, we focus on TEM specimen preparation of different thin films (GaN, Ge₂Sb₂Te₅, TiO₂) and interface structures (GaN/6H-SiC, SrTiO₃/TiO₂, Ge₂Sb₂Te₅/Si) using a combination of FIB with a focused low-energy Ar ion polishing. The results show that this combination enables the routine preparation of high quality TEM lamellae with a smooth surface and uniform thickness, even at the interface region between two different materials and over a lateral range of several micrometres. The prepared lamellae exhibit less surface damage and are well suited for atomic-resolution Cs-corrected STEM/TEM imaging at medium and low accelerating voltages. These results are in a good agreement with Monte Carlo simulations performed by the Stopping and Range of Ions in Matter (SRIM) software.

© 2015 Elsevier Ltd. All rights reserved.

1. Introduction

For high-resolution aberration-corrected (Cs-corrected) scanning transmission electron microscopy (STEM) the quality of prepared TEM specimens is crucial, since the image resolution and the quality of TEM data depend essentially on the thickness and surface quality of the TEM lamella. Depending on the accelerating voltages used for TEM work, TEM specimens should be as thin as 10 nm or less for low voltage TEM work (80 kV and lower) and they have to be as thin as 30 nm or less for medium voltage TEM work (e.g., 300 kV). Nowadays, the widely used focused Ga ion beam (FIB) preparation technique with standard FIB configuration cannot be employed in the fabrication of high-quality TEM specimens with uniform thicknesses of less than 30 nm over several micrometres width. The specimens after FIB preparation are often too thick (>50 nm even after the 5 keV low voltage thinning step) for TEM studies and are produced with strong ion implantation damage near the free surfaces. In particular, FIB preparation of cross-sections from interfaces for atomic resolution Cs-corrected TEM and energy-loss electron spectroscopy (EELS) studies is often a difficult task. Noticeable, thin TEM samples with thicknesses between 10 and 20 nm for such TEM investigations can be prepared by using a modified FIB technique [1,2]. However, it requires either a special rotation-tilt holder or a well aligned FIB system at low Ga ion energies (1 and 2 keV) [2]. In addition, damage and amorphization of the specimen surface induced by ion irradiation during the milling process occur.

This damaged layer is a disorder of the original structure of the sample surface. The damaged or amorphized volume can be removed by chemical wet polishing after FIB milling [3,4]. However, chemical wet polishing methods are material dependent and are difficult or even impossible to use for complex multi-phase or multilayered TEM specimens. To overcome these disadvantages of the FIB preparation, a low-energy Ar ion milling post FIB lamella treatment can be used [4–6].

In the present work, we focus on FIB lamella preparation of different thin films (GaN, Ge₂Sb₂Te₅, TiO₂) and interface structures (GaN/6H-SiC, SrTiO₃/TiO₂, Ge₂Sb₂Te₅/Si) using a combination of FIB with a focused low-energy Ar ion polishing. The results show that this combination enables the routine preparation of high quality TEM specimens with parallel surfaces and thicknesses of less than 20 nm over a range of several micrometres. The prepared specimens exhibit less surface damage and are well suited for atomic resolution Cs-corrected S/TEM work at 300 kV and 80 kV accelerating voltages. These results are in good agreement with simulations performed using the Stopping and Range of Ions in Matter (SRIM) software.

2. Experimental

For FIB lamella preparation the standard FIB cross-section lift-out method in a Zeiss Auriga Dual Beam system was used. The FIB lamellae were cut out using a Ga ion beam with a beam energy of 30 keV and a beam current of 4 nA. A nanocrystalline Pt layer was deposited by FIB from an organic precursor in order to protect the surface of the lamella from ion damage and implantation induced by high-energy ion irradiation. Subsequently, the lamellae were processed to electron transparency

* Corresponding author.

E-mail address: andriy.lotnyk@iom-leipzig.de (A. Lotnyk).

with a 5 keV Ga ion beam at a beam current of 50 pA and a milling time of 3 min per side. The angle between the specimen surface and the ion beam during the FIB milling was $\sim 1^\circ$ for 30 keV and 3° for 5 keV. After the FIB preparation, the TEM lamellae were further treated by focused low-energy Ar ion milling with ion energies of less than 2 keV at a beam currents of either 45 pA or 110 pA in a NanoMill (Fischione) system. The FIB lamellae were milled from the top and bottom sides by adjusting a milling angle of $+10^\circ$ and -10° , respectively, at a static beam orientation scanned over a $10 \times 20 \mu\text{m}$ window. The typical spot size of the ion beam in the NanoMill system given by the manufacture varies between 1 and $4 \mu\text{m}$, depending on the ion energy. Fig. 1(a) shows a SEM image of a FIB lamella mounted on a FIB grid. The indication of the incidence direction for Ar ion beam is presented in Fig. 1(b) and is named front-side polishing (from the Pt side). The ion milling from the side marked as “thick area” in Fig. 1(b) is called a back-side ion beam polishing.

In the final last step, the TEM lamellae were treated for 10 min in a Solarus plasma cleaner using a gas mixture of H_2/O_2 in order to remove organic contaminations from the specimen surface.

The thicknesses of the TEM specimens were measured using energy filtered TEM (EFTEM) by acquiring thickness maps from different specimen areas. The mean free path of electrons in the studied materials was calculated by using the plug-in “mean free path calculator” implemented into the Gatan digital micrograph software. Surface topography of TEM specimens was studied by atomic force microscopy (AFM) in non-contact mode using a Si cantilever with a nominal tip radius of 7 nm. The simulations on interaction of ions with matter were performed by using the SRIM software [7]. In all calculations, 10^5 incident ions were taken into account with full damage cascades.

The investigated TEM specimens were prepared from epitaxial GaN thin films grown on a 6H-SiC (0001) by ion-beam assisted MBE [8–10] and from $\text{Ge}_2\text{Sb}_2\text{Te}_5$ thin films produced on Si substrates by pulsed laser deposition [11,12] as well as from TiO_2 thin films deposited by electron beam evaporation on SrTiO_3 (001) substrates [13]. The focused

low-energy argon ion milling of the $\text{Ge}_2\text{Sb}_2\text{Te}_5$ material was done under liquid N_2 cooling.

S/TEM observations were performed with a probe Cs-corrected Titan³ G2 60–300 microscope equipped with high-angle annular dark-field (HAADF-), bright-field (BF-), ADF, annular BF-STEM and Super-X EDX detectors as well as with a Gatan imaging post-column energy filter (GIF Quantum). The TEM was operated at 300 kV accelerating voltage.

3. Results and discussion

3.1. SRIM simulations

The formation of a damaged (amorphous) layer during the ion milling process is related to the generation of surface defects, e.g., point defects, produced due to the interaction of ions with a specimen surface. This process can be understood by Monte-Carlo simulations implemented into SRIM package. The milling processes in FIB and the focused low-energy ion milling in the NanoMill were simulated using the parameters mentioned in the experimental section. It should be noted that the SRIM simulations do not take into consideration temperature or channelling effects. SRIM simulations for GaN and TiO_2 materials regarding the distribution of vacancies generated per impinging ion and nanometre are shown in Fig. 2(a) and (b), respectively. It can be seen that low-energy Ar ions produce much less implantation and point defects than the high-energy Ga ions. The generated defects by the low-energy Ar milling are located close to the specimen surface forming a thin damaged (amorphous) surface layer. In contrast, high-energy Ga ions produce more defects and thus, a thicker damaged (amorphous) surface layer can be formed after the high-energy Ga ion milling. It should be noted that qualitatively similar results regarding the distribution of vacancies generated per impinging ion and nanometre were obtained for other material systems studied in this work.

The amorphous layer is supposed to be of the same composition as the target material since the ion-matter interaction destroys the crystalline structure of the material forming a disordered surface layer of the same material. This process is a well documented process [14–16]. The implantation of the ion into the disordered amorphous layer is also expected. However, the amorphization depends on the nature of the materials [15–17]. Therefore, the ion beam induced amorphous layer is not formed on the surface of the metallic compounds since the metallic bonds will reform in the lattice.

3.2. Estimation of amorphous surface layer and HRTEM imaging

The formation of a thin damaged surface layer after focused low-energy Ar ion milling is in agreement with experimental results. Fig. 3(a) and (b) shows high-resolution TEM images (HRTEM) of a GaN thin film prepared by low-energy Ar ion milling with an ion energy of 1.6 keV. The damaged/amorphization sidewall layer on Pt and GaN is uniform and was measured to be 3 nm. It should be noted that the real thickness of the amorphous layer has to be calculated from the width of the measured amorphous edge if the shape of the edge is known [18]. In order to re-calculate the real thickness of the amorphous layer covering the sample faces, the measured amorphous edge width should be multiplied with the sine of the half-opening angle of the sample edge. Since, the thickness of TEM specimens measured by EFTEM thickness maps along x- and y-directions did not change dramatically at the regions of interests (see results below), it can be assumed that the TEM specimens are produced with nearly parallel surfaces. Thus, the thickness of the amorphous layer covering the crystalline part of the specimen can be approximated to ~ 2.2 nm which is in a good agreement with SRIM simulations whereas the penetration depth of Ar ions into GaN was estimated to be ~ 3 nm. Notably, this amorphous layer is also present on the specimen top and bottom surfaces. Moreover, the amorphous layer induces an inhomogeneous image contrast and influences the resolution of the atomic columns of the GaN lattice.

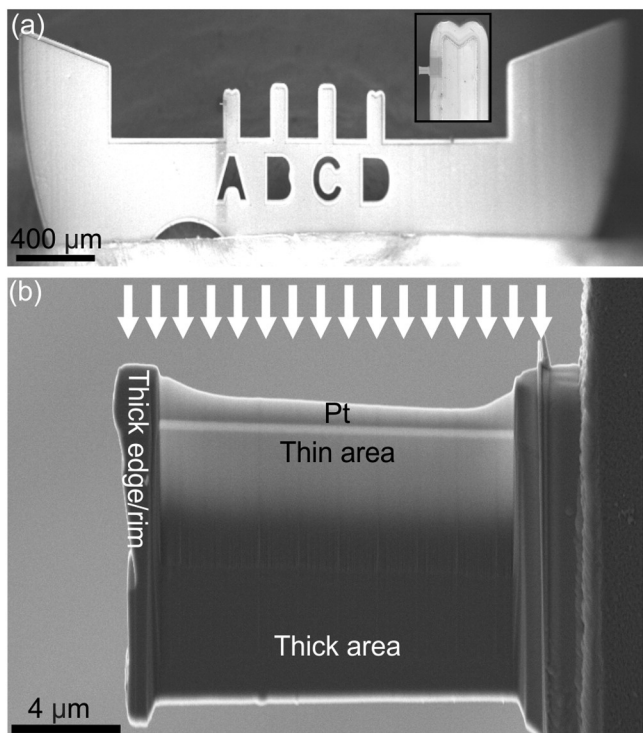


Fig. 1. (a) SEM image of a FIB lamella fixed onto a FIB grid. The lamella is mounted on a post A. (b) SEM micrograph of a FIB prepared specimen with the indication for the incidence direction of Ar beam, Pt layer, thin and thicker areas. Inset in (a) shows a magnified image of the lamella with FIB post.

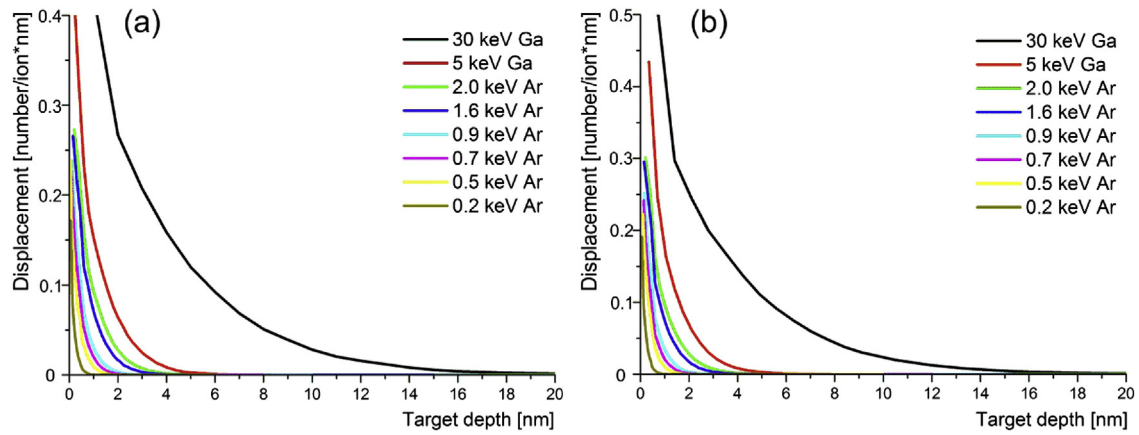


Fig. 2. Total number of generated defects per impinging ion as a function of (a) GaN and (b) TiO_2 material depths. The angles between the specimen surface and the ion beam used for the simulations are $\sim 1^\circ$ for 30 keV Ga, 3° for 5 keV Ga and 10° for 0.2–2 keV Ar.

The thickness of the surface amorphous layer can be even reduced to a value of less than 1 nm by using Ar ion beam with lower energies. Fig. 4(a) shows HRTEM micrograph of GaN thin film prepared by focused low-energy Ar ion milling with an ion energy of 200 eV. The Pt protective layer is intact in Fig. 3(b). The damaged (amorphization) sidewall layer on the Pt layer is uniform and was measured to be less than 0.5 nm (see Fig. 4(b)) whereas the penetration depth of Ar ions into the GaN material was estimated to be approximately 1 nm from the SRIM simulations. Due to the small thickness of the surface amorphous layer, the HRTEM image contrast in Fig. 4(a) and (c) is improved compared to the HRTEM image contrast of Fig. 3(b). In addition, the TEM image contrast is also uniform over the whole image. All atomic columns in GaN and 6H-SiC materials are well resolved. Moreover, the contrast at the GaN/SiC interface is also homogenous. The latter is a preferable image condition for structural solution from e.g., quantitative electron exit wave analysis and for quantitative comparison of experimental and simulated HRTEM images.

It is worth to note that the formation of natural oxide and carbonaceous contaminations in air as well as during plasma cleaning on many surfaces is also possible. The thickness of this “amorphous” layer is a kinetic limiting process and material dependent. In the presented experiments, the formation of such (thick) amorphous layer was not

observed. Consequently, the observed amorphous layer in this work is mainly due to ion beam damages.

Redeposition of material from a TEM specimen support during a broad ion milling (beam size of several hundreds of micrometres) is a well-known problem. Due to the broad beam size, the ion beam can hit a TEM support and the re-sputtered material from the support can be found on the surface of a TEM specimen during TEM work. Thus, the redeposited layer can hinder image and chemical analysis. On the other hand, redeposition during a focused low-energy Ar ion milling is minimized by careful orientation of the TEM lamella with respect to the FIB support grid. Because the lamella and ion beam diameter are of the same relative size, there are no Ar ions hitting the TEM support. In the present work, no redeposition on the TEM specimen surfaces was observed in the studied specimens.

The redeposition from the surface of the lamellae itself is usually reduced by using grazing incidence angle [15,19]. This also has an advantage in improving the surface topography (see also AFM results below). Thus, the surface has less “hills” where the local redeposition may occur. Moreover, the redeposition may also appear at the thicker rims/edges of the FIB lamellae (see Fig. 1(b)) or during back-side ion beam polishing. In this work, no such redeposited layers were observed during TEM measurements due possibly to its small thickness.

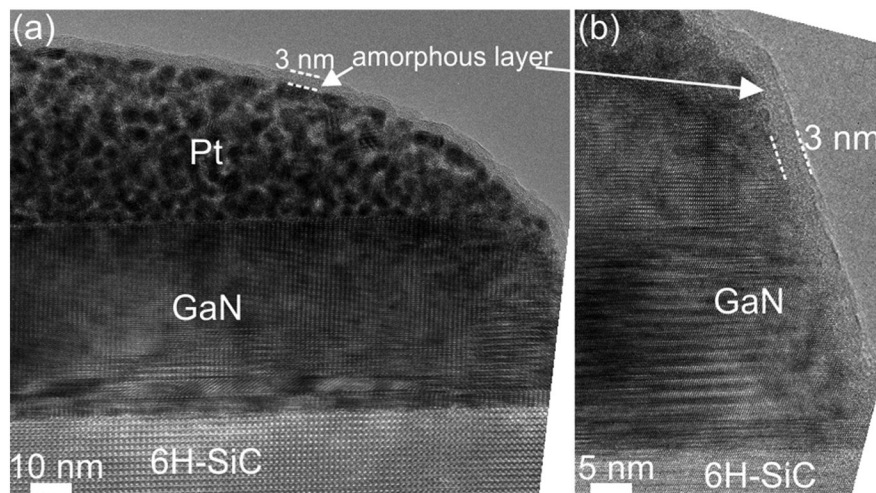


Fig. 3. HRTEM images of FIB prepared specimen after low-energy Ar ion milling with an ion beam energy of 1.6 keV. The TEM specimen thickness of GaN is approximately 40 nm whereas the specimen thickness of SiC is approximately 51 nm.

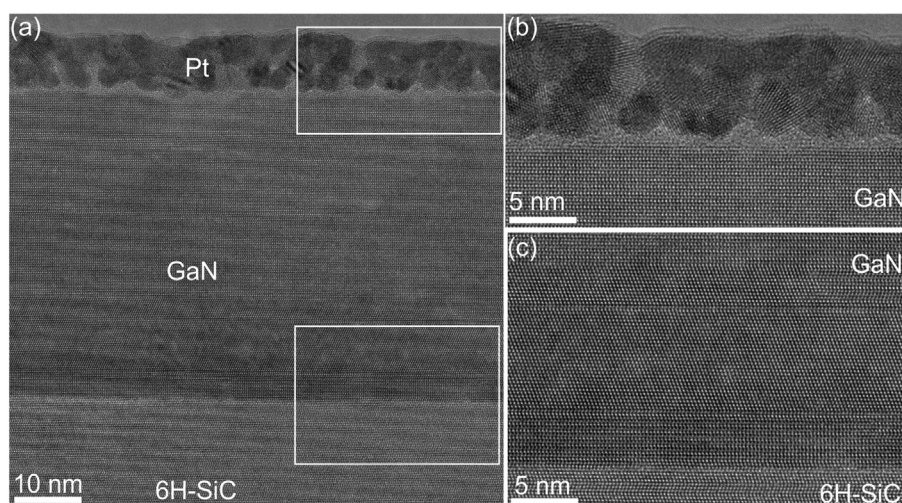


Fig. 4. HRTEM images of FIB prepared specimen after focused low-energy Ar ion milling at a beam energy of 200 eV. The image contrast is uniform in (a), (b) and (c). The atomic columns at the GaN/SiC interface and planar defects in GaN are distinctly resolved in (c). The TEM specimen thickness is 10 nm for the GaN material and is 15 nm for the 6H-SiC material.

3.3. Thickness measurements and curtaining effect

Post-treatment of FIB lamellae, as described above, resulted always in an improved quality of the TEM specimen surfaces with uniform thickness over large specimen areas as well as at the film/substrate interface. However, several treatment steps at different ion energies were necessary to prepare TEM lamella with a desired final specimen thickness. It should be noted that the accuracy of the thickness measurements by EELS is 20% since the values of the inelastic mean free paths (mfp) are not well known for many compounds. The mfp should therefore be identified experimentally since the error in the thickness measurements based on the parameterised approach of Malis et al. [20] can exceed 20% [21].

Fig. 5(a) and (b) shows EFTEM thickness maps of GaN/6H-SiC specimen acquired after the focused low-energy Ar ion milling at a beam energy of 1600 eV and 900 eV, respectively. After the treatment at an ion beam energy of 900 eV, the mean thickness of the TEM specimen was reduced from 40 nm to 20 nm (see Fig. 5(d) and (e)). In addition, a slight variation in the thickness of the TEM specimen due to different sputtering yields of the GaN and 6H-SiC materials can be determined at the interface region (see Fig. 5(c) and (f)).

Due to uncertainties in the measurements of mfp, the roughness of the TEM lamellae and the height of the step at the GaN–SiC interface were additionally studied by AFM. Fig. 6 shows an AFM image of the TEM specimen after the focused low-energy Ar ion milling at a beam energy of 200 eV. The measured root mean square roughness (RMS) along the GaN and SiC materials is less than 0.5 nm while the RMS along the GaN–SiC interface is less than 0.2 nm in Fig. 6. This highlights the uniform thickness of the TEM specimen, especially at the GaN–SiC interface. Consequently, the projection artefacts or blurring at the interface during TEM/STEM investigation are reduced. Notably, the difference in the step height at the interface is much smaller than measured by EELS. Thus, iterative focused low-energy ion milling in combination with thickness measurements by EFTEM thickness maps always resulted in a high-quality, thin and very smooth TEM specimen. However, careful adjustment of the ion milling parameters such as milling time, ion energy and ion beam current is necessary for reliably reproducible TEM specimen preparation.

The thickness measurements after focused low-energy Ar ion milling allow the determination of milling rate for different materials. The milling rates are dependent on the ion beam current, ion beam energy, specimen temperature and the specific incidence angle. The sputtering

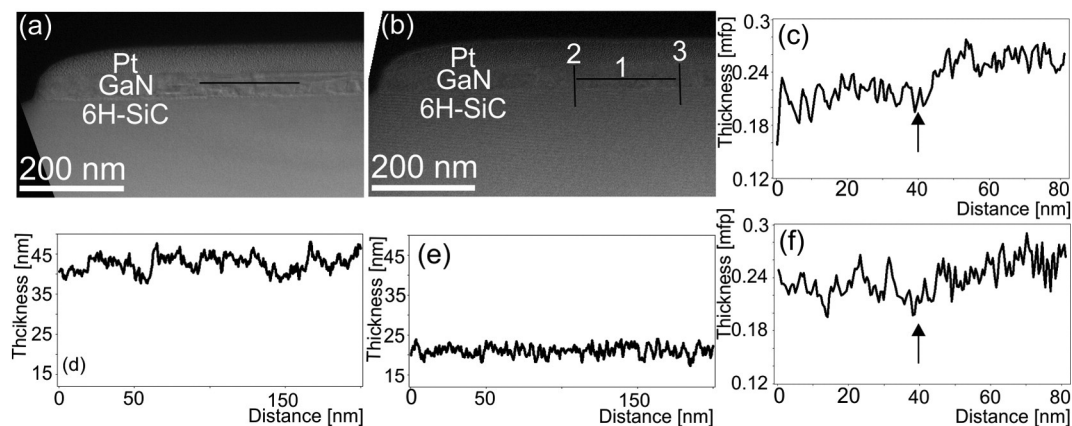


Fig. 5. GaN thin film on 6H-SiC prepared by FIB with post processing by focused low-energy Ar ion milling. (a) and (b) EFTEM thickness maps of TEM specimens prepared by the low-energy ion milling with ion energies of 1600 eV and 900 eV, respectively. The thickness profile in (c) was taken along the line marked by 2 in (b). The thickness profile in (d) was taken along the line marked in (a). The thickness profiles in (e) and (f) were taken along the lines marked by 1 and 3 in (b), respectively. The arrows in (c) and (f) mark the GaN/SiC interface. The mean free path (mfp) of electrons in GaN and SiC materials at an acceleration voltage of 300 kV is 94 nm and 115 nm, respectively.

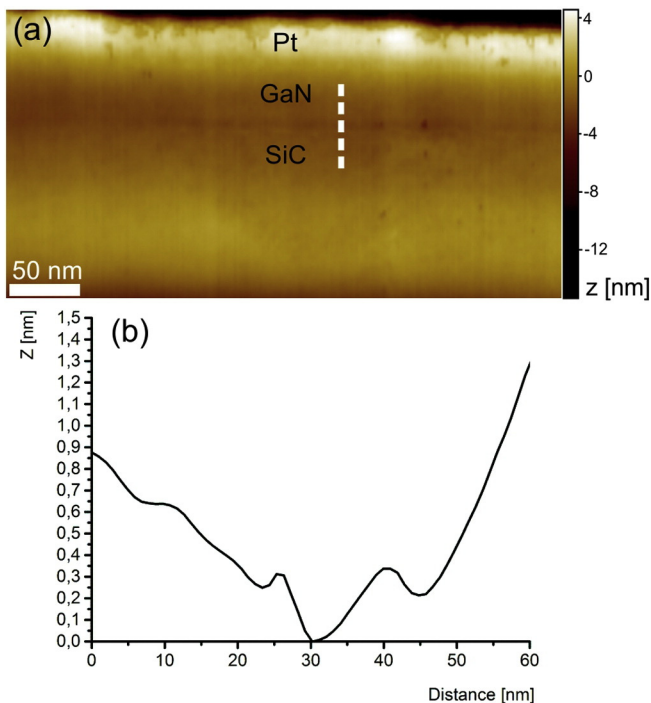


Fig. 6. (a) AFM topography image of a FIB lamella after focused low energy ion polishing. (b) Line profile taken along the dashed line in (a). This TEM specimen was prepared by low-energy back-side ion beam polishing.

rate for GaN material at a beam current of 110 pA and an ion beam energy of 900 eV at room temperature was determined to be ~ 0.85 nm/min, whereas this rate is 0.15 nm/min for an ion beam energy of 500 eV. On the other hand, the sputtering rates for $\text{Ge}_2\text{Sb}_2\text{Te}_5$ material at an ion beam current of 110 pA processed under liquid N_2 cooling were estimated to be ~ 0.8 nm/min for an ion energy of 900 eV and ~ 0.2 nm/min for an ion energy of 500 eV. The etching rates for $\text{Ge}_2\text{Sb}_2\text{Te}_5$ at a beam current of 45 pA under liquid N_2 cooling were found to be ~ 0.6 nm/min for an ion energy of 900 eV and ~ 0.05 nm/min for an ion energy of 500 eV. It should be noted that the ion beam current was determined with an accuracy of $\pm 10\%$. Although the sputtering rate for different materials should be determined experimentally in further detail, the above presented data could be a good starting point for every focused low-energy milling of a FIB lamella. In addition, the estimated above sputtering rates at a beam current of 110 pA are in a good agreement with the reported sputtering rate of 0.7 nm/min at a beam current of 120 pA for oxide materials ($\gamma\text{-Ga}_2\text{O}_3$ thin film, MgO substrate) and semiconductors ((Zn, Cr)Te thin film, GaAs substrate) [22]. It is worth to mention that the sputtering rate also critically depends on the actual incidence angle of the ion beam with respect to the specimen surface. Variations in the mounting of a FIB grid into the NanoMill sample holder may lead to different measured sputtering rates.

A high surface roughness in multiphase systems and layers of different sputtering yields can result in preferential milling and can lead to preparation artefacts like curtain effects. Since, the FIB lamella is not rotated or tilted during the focused low-energy Ar ion milling, curtaining is an issue during the milling process. The problem becomes increasingly troublesome for thin TEM specimens. Fig. 7 shows a thickness map of a GaN/SiC specimen where vertical stripes are seen as light and dark contrasts in the image. However, this preparation artefact can be reduced by choosing an appropriate polishing geometry in NanoMill, e.g., using back-side ion polishing [23] as shown in Figs. 5 and 6. Another approach for minimization of the curtaining effects is to spread the ion beam, thus increasing the overlap between scanning raster spots.

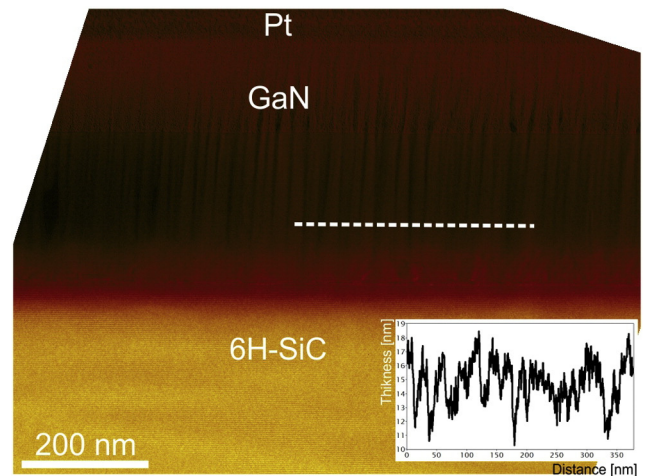


Fig. 7. EFTM thickness map of GaN thin film grown on SiC substrate. The insert shows a thickness line profile taken along the dashed line.

3.4. Atomic-resolution STEM results

The reduction of TEM specimen thickness and surface damaged (amorphous) layer thickness resulted always in a significant improvement of signal to noise (S/N) ratio upon STEM image acquisition. Fig. 8 shows atomic-resolution HAADF-STEM images of a typical interface between a TiO_2 (anatase) thin film and a SrTiO_3 substrate. Due to the specimen thickness of 60 nm and a thick damaged layer the atomic columns at the $\text{TiO}_2/\text{SrTiO}_3$ interface appear blurred in Fig. 8(a). After a focused low-energy ion milling step the specimen thickness was reduced to 20 nm and the specimen quality was improved significantly. As a result, the atomic columns at the $\text{TiO}_2/\text{SrTiO}_3$ interface can be distinctly resolved in Fig. 8(b) and thus, the interface structure can be solved. The interface between the TiO_2 thin film and the SrTiO_3 substrate is rough. However, there is no interfacial or amorphous layer at the $\text{TiO}_2/\text{SrTiO}_3$ interface. It should be noted that the image presented in Fig. 8(b) is a raw Cs-corrected HAADF-STEM image without the application of any

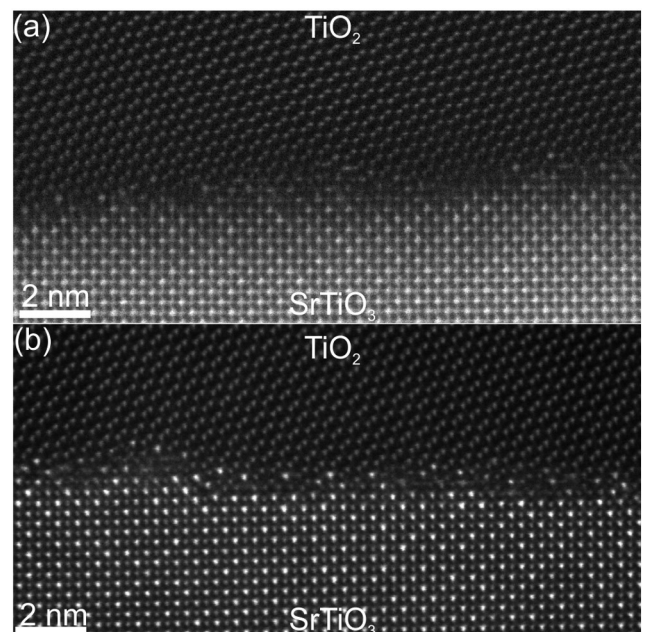


Fig. 8. Atomic-resolution HAADF-STEM images of the TiO_2 (anatase)/ SrTiO_3 interface. TEM specimen thickness is 60 nm in (a) and is 20 nm in (b).

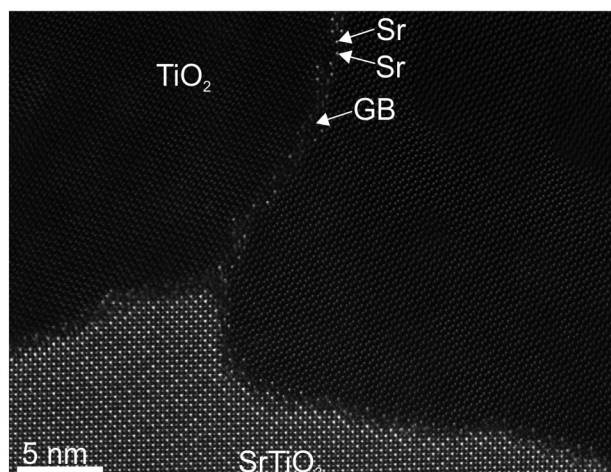


Fig. 9. (a) Atomic-resolution HAADF-STEM image of (a) the $\text{TiO}_2/\text{SrTiO}_3$ interface and (b) the interface region between two TiO_2 grains decorated by Sr atoms. The grain boundary (GB) is decorated by Sr atoms.

imaging filters. In addition, both images in Fig. 8(a) and (b) were acquired with the same dwell time per pixel and with the same image size as well as identical detector settings in order to eliminate the influence of the acquisition time on S/N ratio in the STEM images.

A uniform TEM specimen thickness over a wide area allows studying different areas in the FIB lamella. Due to uniform specimen thickness, projection artefacts are minimized and the real structure of grain boundaries and interfaces can be studied. Fig. 9 shows an atomic-resolution HAADF-STEM image of the $\text{TiO}_2/\text{SrTiO}_3$ interface and the grain boundary between two TiO_2 grains. It should be noted that the qualitative interpretation of HAADF-STEM micrographs is quite straightforward, since the image intensities are proportional to the atomic number according to $I \sim Z^{1.8}$ and the atomic columns with higher average Z number therefore appear brighter than the columns with lower average Z number in the HAADF images. The Z number of Sr is 38 whereas the Z number of Ti is 22 and of oxygen is 6. Thus, the bright dots in Figs. 8 and 9 are Sr atomic columns whereas the darker spots are Ti/O atomic columns. In Fig. 9, the out-diffusion of Sr atoms from the SrTiO_3 substrate was found. The Sr atoms are in-diffused into the grain boundary between two TiO_2 grains. Interestingly, no in-diffusion of Sr into the TiO_2 lattice was observed (see also Fig. 8), even though the

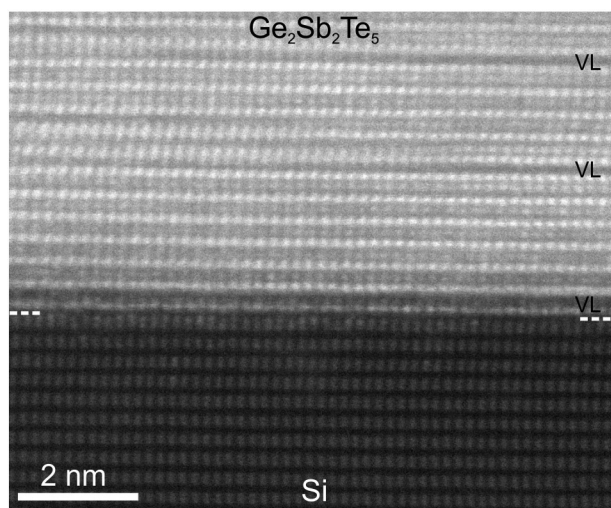


Fig. 10. High-resolution HAADF-STEM image of the $\text{Ge}_2\text{Sb}_2\text{Te}_5/\text{Si}$ interface. The dashed lines mark the interface. The positions of vacancy layers are marked by “VL”.

TiO_2 (anatase) thin film was grown by e-beam evaporation of TiO_2 at a substrate temperature of 900 °C.

Another example of a successfully post-treated FIB lamella with focused low-energy Ar ions is given in Fig. 10. The figure shows a raw atomic-resolution HAADF-STEM image of the interface between $\text{Ge}_2\text{Sb}_2\text{Te}_5$ thin film with hexagonal structure and the Si substrate. The $\text{Ge}_2\text{Sb}_2\text{Te}_5$ thin film was produced by pulsed laser deposition of a $\text{Ge}_2\text{Sb}_2\text{Te}_5$ target on Si (111) without native oxide at a substrate temperature of 185 °C. The initial thickness of the TEM specimen after the FIB preparation was more than 100 nm. The thickness of the TEM lamella was reduced to 30 nm over a wide area after polishing with a focused low-energy Ar ion beam. Remarkably, due to the improvement of the S/N ratio through the reduction of damaged (amorphous) layer thickness, the atomic columns of different elements in different materials as well as intrinsic vacancy layers are distinctly resolved in the atomic-resolution HAADF-STEM image in Fig. 10. The bright dots in the $\text{Ge}_2\text{Sb}_2\text{Te}_5$ thin film in Fig. 10 represent Te atomic columns while the darker spots show mixed Ge/Sb atomic columns. Thus, the atomic structure of the $\text{Ge}_2\text{Sb}_2\text{Te}_5/\text{Si}$ interface can be directly evaluated from the HAADF-STEM image. The $\text{Ge}_2\text{Sb}_2\text{Te}_5/\text{Si}$ interface is sharp without the formation of any interfacial layers between the Si substrate and the first Te atomic layer.

The results on atomic-resolution imaging of GaN thin films and the GaN/SiC interface can be found in Refs. [8–10].

4. Conclusions

The combination of focused high-energy ion milling with focused low-energy Ar ion milling enables the routine preparation of high quality TEM lamellae from different materials and interfaces with smooth surface and uniform thickness of TEM specimens even at the interface regions. The TEM specimens prepared by this approach are well suited for atomic-resolution Cs-corrected S/TEM imaging and atomic EDX and EELS analysis at medium and low accelerating voltages. The thickness of the amorphous/damaged surface layer can be reduced below 1 nm by low energy ion milling resulting in a homogeneous image contrast in TEM and STEM images which is a prerequisite condition for quantitative image analysis. However, a certain amount of surface damage cannot be avoided even by using low-energy Ar ion milling as the last preparation step. The preparation artefacts such as curtaining effects caused by the low-energy focused ion beam can be successfully reduced by using back-side ion polishing.

Although careful adjustment of the milling parameters is still necessary for successful TEM specimen preparation, the presented combination of the focused high-energy Ga and low-energy Ar ion milling technique can be generally applicable for various materials with fully reproducible results. Since the combination of site-specific FIB specimen preparation and failure analysis methods, e.g., electron beam induced current (EBIC), is nowadays possible within the same instrument, the post FIB focused low-energy Ar ion milling opens up the possibility to re-polish the lamella without losing the faulty region and damaging of the lamella surface by the high-energy ion beam. This will enable better S/TEM imaging and chemical analysis of failed devices.

Acknowledgements

The financial support of the European Union and the Free State of Saxony (LenA project, project No. 100074065) is greatly acknowledged. We would like to thank Mrs. A. Mill (IOM Leipzig) for her assistance in the TEM specimen preparation by FIB.

References

- [1] L. Lechner, J. Biskupek, U. Kaiser, Improved focused ion beam target preparation of (S)TEM specimen—a method for obtaining ultrathin lamellae, *Microsc. Microanal.* 18 (2012) 379–384.

- [2] M. Schaffer, B. Schaffer, Q. Ramasse, Sample preparation for atomic-resolution STEM at low voltages by FIB, *Ultramicroscopy* 114 (2012) 62–71.
- [3] N.I. Kato, Y. Kohn, H. Saka, Side-wall damage in a transmission electron microscopy specimen of crystalline Si prepared by focused ion beam etching, *J. Vac. Sci. Technol. A* 17 (1999) 1201.
- [4] T. Mehrkens, S. Bley, P.V. Satyam, A. Rosenauer, Optimization of the preparation of GaN-based specimens with low-energy ion milling for (S)TEM, *Micron* 43 (2012) 902–909.
- [5] A. Barna, B. Pecz, M. Menyhard, TEM sample preparation by ion milling/amorphization, *Micron* 30 (1999) 267–276.
- [6] N. Miyajima, C. Holzapfel, Y. Asahara, L. Dubrovinsky, D.J. Frost, D.C. Rubie, M. Drechsler, K. Niwa, M. Ichihara, T. Yagi, Combining FIB milling and conventional argon ion milling techniques to prepare high-quality site-specific TEM samples for quantitative EELS analysis of oxygen in molten iron, *J. Microsc.* 238 (2010) 200–209.
- [7] J. Ziegler, J. Biersack, U. Littmark, *The Stopping and Range of Ions in Solids*, Pergamon Press, New York, 1996.
- [8] D. Poppitz, A. Lotnyk, J.W. Gerlach, B. Rauschenbach, Microstructure of porous gallium nitride nanowall networks, *Acta Mater.* 65 (2014) 98–105.
- [9] A. Lotnyk, D. Poppitz, J.W. Gerlach, B. Rauschenbach, Direct imaging of light elements by annular dark-field aberration-corrected scanning transmission electron microscopy, *Appl. Phys. Lett.* 104 (2014) 071908.
- [10] D. Poppitz, A. Lotnyk, J.W. Gerlach, J. Lenzner, M. Grundmann, B. Rauschenbach, An aberration-corrected STEM study of structural defects in epitaxial GaN thin films grown by ion beam assisted MBE, *Micron* 73 (2015) 1–8.
- [11] U. Ross, A. Lotnyk, E. Thelander, B. Rauschenbach, Direct imaging of crystal structure and defects in metastable Ge₂Sb₂Te₅ by quantitative aberration-corrected scanning transmission electron microscopy, *Appl. Phys. Lett.* 104 (2014) 121904.
- [12] E. Thelander, J.W. Gerlach, U. Ross, A. Lotnyk, B. Rauschenbach, Low temperature epitaxy of Ge–Sb–Te films on BaF₂ (111) by pulsed laser deposition, *Appl. Phys. Lett.* 105 (2014) 221908.
- [13] A. Lotnyk, S. Senz, D. Hesse, Epitaxial growth of TiO₂ thin films on SrTiO₃, LaAlO₃ and yttria-stabilized zirconia substrates by electron beam evaporation, *Thin Solid Films* 515 (2007) 3439–3447.
- [14] A. Barna, B. Pécz, M. Menyhard, Amorphisation and surface morphology development at low-energy ion milling, *Ultramicroscopy* 70 (1998) 161–171.
- [15] D.J. Barber, Radiation damage in ion-milled specimens: characteristics, effects and methods of damage limitation, *Ultramicroscopy* 52 (1993) 101–125.
- [16] Y. Huh, K.J. Hong, K.S. Shin, Amorphization induced by focused ion beam milling in metallic and electronic materials, *Microsc. Microanal.* 19 (S5) (2013) 33–37.
- [17] J. Yua, J. Liub, J. Zhanga, J. Wu, TEM investigation of FIB induced damages in preparation of metal material TEM specimens by FIB, *Mater. Lett.* 60 (2006) 206–209.
- [18] M.J. Süess, E. Mueller, R. Wepf, Minimization of amorphous layer in Ar ion milling for UHR-EM, *Ultramicroscopy* 111 (2011) 1224–1232.
- [19] A. Strecker, J. Mayer, B. Baretzky, W. Eigenthaler, Th. Gemming, R. Schweinfest, M. Rühle, Optimization of TEM specimen preparation by double-sided ion beam thinning under low angles, *J. Electron Microsc.* 48 (3) (1999) 235–244.
- [20] H. Meltzman, Y. Kauffmann, P. Thangadurai, M. Drozdov, M. Baram, D. Brandon, W.D. Kaplan, An experimental method for calibration of the plasmon mean free path, *J. Microsc.* 236 (2009) 165–173.
- [21] T. Malis, S.C. Cheng, R.F. Egerton, EELS log-ratio technique for specimen-thickness measurement in the TEM, *J. Electron Microsc. Tech.* 8 (1988) 193–200.
- [22] M. Mitome, Ultrathin specimen preparation by a low-energy Ar-ion milling method, *Microscopy* 62 (2013) 321–326.
- [23] S.M. Schwarz, B.W. Kempshall, L.A. Giannuzzi, M.R. McCartney, Avoiding the curtaining effect: backside milling by FIB INLO, *Microsc. Microanal.* 9 (Suppl. 2) (2003) 116–117.